# Numerical Analysis of 3D Subsurface Crack Propagation in Large Slewing Bearing

**R. Potočnik[1] and J. Flašker[2] and S. Glodež[3]**

[1] Faculty of Mechanical Engineering, University in Maribor, Smetanova 17, SI-2000 Maribor, Slovenia, roki.potocnik@uni-mb.si
[2] Faculty of Mechanical Engineering, University in Maribor, Smetanova 17, SI-2000 Maribor, Slovenia, joze.flasker@uni-mb.si
[3] Faculty for Natural Sciences and Mathematics, University in Maribor, Koroška cesta 160, SI-2000 Maribor, Slovenia, srecko.glodez@uni-mb.si

***ABSTRACT.*** *This paper presents a numerical calculation procedure for determination of subsurface crack propagation in a large slewing ball bearing. In the first step, a maximum contact force on the bearing raceway is obtained by means of analytical expressions, where the Hertzian contact theory is used. In the second step a 3D finite element model of the raceway segment and the contact load is simulated, and the subsurface stresses and strains are obtained. At the time being the contact load on the raceway is approximated by Hertzian pressure distribution as calculated in the previous step. Depth dependent elasto-plastic material properties are used in the finite element model of the raceway. In the third step a submodel with the elliptical crack is made and the crack intensity factors are calculated. The linear elastic fracture mechanics theory is used for this purpose. Due to complexity of a problem at this very moment the finite element analysis does not provide sufficient results. However, it seams that in near future an improved and fine-tuned finite element model will be suitable for characterization of subsurface crack propagation analysis.*

## INTRODUCTION

Slewing bearings are machine elements which enable relative rotation of two structural parts. They are widely used in the construction of transport devices (cranes, transporters, turning tables, etc.), wind turbines production and other fields of mechanical engineering. Slewing bearings can accommodate axial and radial forces and tilting moment loads acting either singly or in combination and in any direction. Some typical loads are shown in Figure 1.

There are not many publications in the professional literature describing the calculation of maximum contact force on the bearing raceway. There is a simple equation available in the literature [1], but it does not take into account the clearance of the bearing and the precise geometry of the raceways, which result in a relative displacement and rotation of the bearing rings. It is also applicable only in cases when

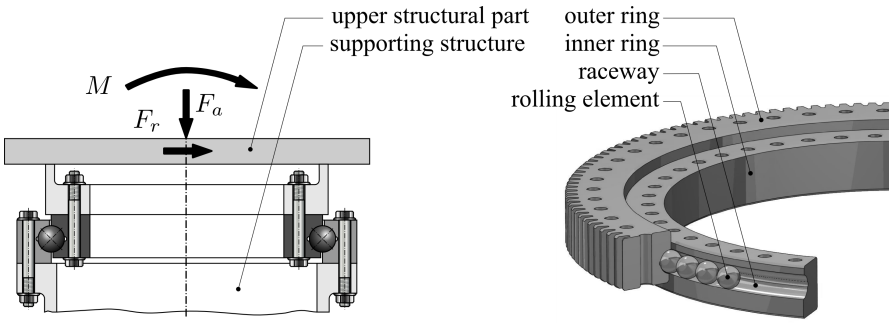

Figure 1. Typical slewing bearing assembly and loading conditions

the *in-plane* loading of the bearing $F_a$, $F_r$ and $M$, such as shown in Figure 1, is applied to the structure. The topic is more thoroughly covered in [2, 3, 4], where analytical models for determination of load distribution on the raceway are presented. In all cases the calculation of load distribution is based on the Hertzian theory of contact and five non-linear algebraic equations of static equilibrium. All models take into consideration the bearing geometry, the non-parallel displacement of the rings, the clearance and the osculation. Furthermore, the investigation presented in [3] also takes into account the deformation of the supporting structure, which is defined by the stiffness matrix obtained on the basis of the finite element analysis.

Likewise, not a lot of information can be found about the crack propagation in large rolling bearings. Quite few authors investigated experimental and/or numerical aspects of crack propagation in similar mechanical parts, such as rails and railroad wheels [5, 6, 7, 8, 9, 10], gears [11, 12, 13, 14, 15] and *small* bearings [16, 17, 18] etc. To our knowledge, there is only one paper [19], which deals exactly with the crack propagation in large rolling bearings. Furthermore, the most numerical investigations mentioned above, except [6, 8, 9, 10], use 2D finite element models for numerical computations. Such models can be used when simulating line contacts, as in case of gears, roller bearings, and, to some extent, in case of railroad wheels or rails. However, they can not be used to simulate crack propagation in ball bearings, since 3D stress and strain fields have to be taken into consideration.

The presented model first shows how to calculate a maximum contact force acting on a rolling element by taking into account external loads acting on a bearing. Later on this maximum contact force is used in a 3D finite element analysis, where subsurface crack propagation is investigated. Submodeling approach is used to reduce the complexity of the problem. At the time being the finite element analysis does not provide good enough results, but this will be improved in the near future. Furthermore, the model is designed completely parametrically, which makes it perfect for parametric analysis.

## CALCULATION OF THE MAXIMUM CONTACT FORCE

A maximum contact force on the bearing raceway is calculated on the basis of the load distribution. The therm *load distribution* stands for the distribution of the contact forces

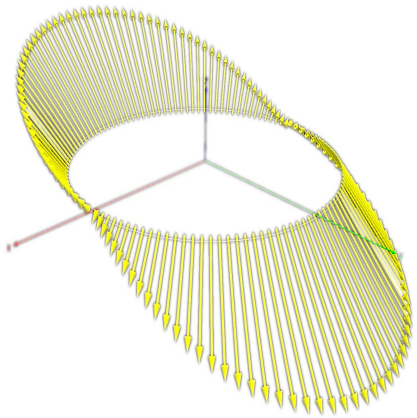

Figure 2. An example of the load distribution on the bearing raceway

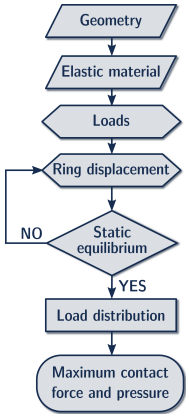


Figure 3. An algorithm for the calculation of the maximum contact force

between the rolling elements and the bearing raceway, which are acting on the bearing raceway. An example of the load distribution is shown in Figure 2.

The algorithm for the calculation of the load distribution and the maximum contact force is shown in Figure 3. The calculation is based on the following assumptions: i) external loads acting on the bearing are in static equilibrium with the contact forces acting on the raceway (see Figure 1), ii) the bearing rings are ideally stiff, thus only elastic contact deformations are taken into account, iii) the procedure for the calculation of the contact forces is based on the Hertzian theory of contact, and iv) the internal ring is fixed, while the external ring can move in $x$, $y$ and $z$ directions and rotate about $x$ and $y$ axes.

The calculation of the contact forces is more thoroughly described in [20], while here only the force and moment equilibrium equations will be written:

$$\begin{aligned} \sum_{j=1}^{n} \left( Q_{1,j} \cdot \vec{e}_{q1,j} + Q_{2,j} \cdot \vec{e}_{q2,j} \right) &= \vec{F} \\ \sum_{j=1}^{n} \left( \vec{r}_{q1,j} \times \vec{Q}_{1,j} + \vec{r}_{q2,j} \times \vec{Q}_{2,j} \right) &= \vec{M} \end{aligned}, \tag{1}$$

where indices 1, 2, $i$ and $o$ represent the adequate direction and geometry, $n$ is a number of the rolling elements, $\vec{e}_{q1,2}$ are unit vectors, which define the direction of the contact forces, and $\vec{r}_{q1,2}$ are direction vectors, which point to the contact point. Since the moment about the $z$ axis is 0, the equation yields a system of 5 equations with 5 unknown variables (displacements and rotations of the bearing ring: $u$, $v$, $w$, $\varphi_x$ and $\varphi_y$), which can be solved using a numerical algorithm for multidimensional root-finding. At the end the maximum contact force $Q_{\max}$, which is later used in the finite element analysis, is calculated as:

$$Q_{\max} = \max\left(Q_j\right) \quad \text{for} \quad j = 1 \ldots n \,. \tag{2}$$

## SUBSURFACE CRACK PROPAGATION ANALYSIS

A subsurface crack propagation analysis is done by means of a finite element analysis, and it consists of two steps. First, a global model, which represents a 3D model of the bearing segment, as shown in Figure 4, is done. This model is used to obtain subsurface stresses, strains and displacements, which are later used as boundary conditions for the submodel, which is shown in Figure 5.

### *Global model*

The geometry of the bearing segment is simplified in such a way that the symmetry can be taken into account. This is done by calculating the equivalent radii of curvatures $r_x$ and $r_y$ as shown in Figure 4. Here $r_c$ represents the curvature radius, $r_{CP}$ represents the radius of the contact point in the plane perpendicular to the axis of the bearing, and $\alpha$ represents the contact angle, i.e. angle between the contact force and the axis of the bearing. The bottom of the model is fixed in all directions.

The bearing segment is divided into layers (see Figure 4), so that the depth-dependent elasto-plastic material properties can be taken into account. Each layer is modelled with the cyclic stress-strain curve characterized by the Ramberg-Osgood equation [21]:

$$\varepsilon_a = \frac{\sigma_a}{E} + \left(\frac{\sigma_a}{K'}\right)^{\frac{1}{n'}} \quad \text{where} \quad K' = \frac{\sigma_f'}{\left(\varepsilon_f'\right)^{b/c}} \quad \text{and} \quad n' = \frac{b}{c}. \tag{3}$$

In the above equation $\varepsilon_a$ and $\sigma_a$ are strain and stress amplitudes, respectively, and $E$, $\sigma_f'$, $\varepsilon_f'$, $b$ and $c$ are Young's modulus of elasticity, fatigue strength coefficient, fatigue ductility coefficient, fatigue strength exponent and Fatigue ductility exponent, respectively. The parameters in equation (3) are obtained on the basis of the available experimental data, i.e. by averaging or by linear regression of the values available from the literature [22, 23]. An assumption, that the material properties for compression and tension are the same has also been made. The raceway has been divided into three layers with different material properties. These layers simulate material changes, which result from the surface hardening.

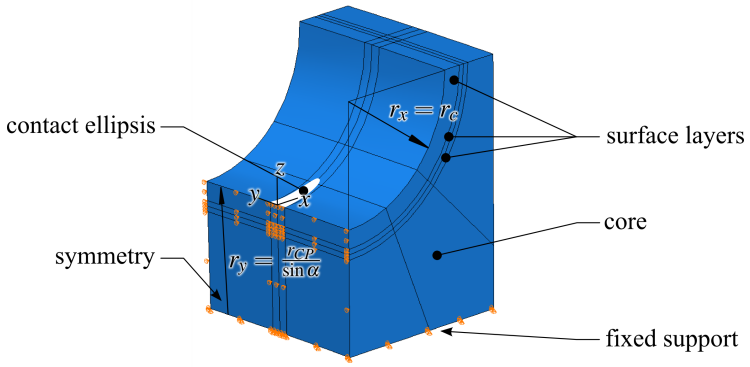


Figure 4. Global finite element model – a model of a bearing segment

The maximum contact load was modelled by Hertzian pressure distribution $p(x, y)$ and Coulomb's friction $q(x, y)$, which are given by the following equations [2]:

$$p(x, y) = p_0 \cdot \sqrt{1 - \left(\frac{x}{a}\right)^2 - \left(\frac{y}{b}\right)^2} \quad \text{and} \quad q(x, y) = \mu \cdot p(x, y), \tag{4}$$

where $p_0$ is the maximum contact pressure on the raceway, $a$ and $b$ are major and minor semi-axes of the contact ellipsis, respectively, and $\mu$ is coefficient of friction. These values are calculated in the calculation of the maximum contact force, as described in the previous section and in [20].

Without a doubt this approach oversimplifies the exact contact conditions. However, it reduces the hardware requirements and computation time significantly, and it was chosen merely to demonstrate the calculation procedure. Moreover, the purpose of the analysis is to evaluate the influence of different parameters on crack propagation, and not to obtain the exact values, which could be used for engineering work.

***Submodel***

The submodel mesh with the crack, and its approximate relation to the global model is shown in Figure 5. The depth of the crack was defined by the maximum subsurface Von Mises stress, which was calculated in the global model. The crack was modelled as two parallel elliptic contact surfaces. The friction between the crack faces was also considered. In the first iteration the aspect ratio of the crack semi-axes was chosen to be $a_{\text{crack}}/b_{\text{crack}} = 1$, and an initial length of the crack semi-axes was approximated by the threshold crack length $a_{\text{th}}$ as described in [12]

At the end the equivalent stress intensity factor $\Delta K_{\text{eq}}$ and the crack extension direction $\theta$ at each crack tip node (see Figure 5) were to be calculated as [24]:

$$\Delta K_{\text{eq}} = \frac{\Delta K_{\text{I}}}{2} + \frac{1}{2}\sqrt{\Delta K_{\text{I}}^2 + 4(1.155\,\Delta K_{\text{II}})^2 + 4(\Delta K_{\text{III}})}, \tag{5}$$

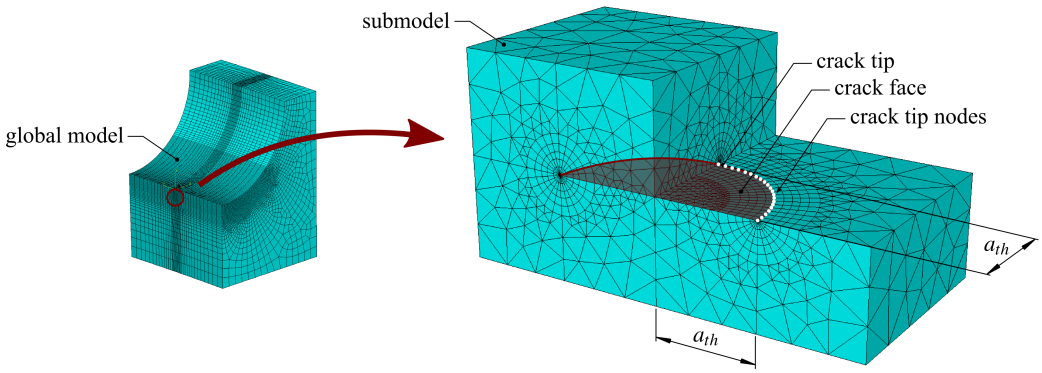


Figure 5. Submodel mesh with the crack

Table 1. Material properties used for the finite element analysis

| | Thickness [mm] | Hardness [HB] | $E$ [MPa] | $\sigma_f'$ [MPa] | $b$ [/] | $\varepsilon_f'$ [/] | $c$ [/] |
|---|---|---|---|---|---|---|---|
| case | 3.5 | 615 | | 2540 | | 0.057 | |
| transition | 1.0 | 445 | 205 | 2040 | – 0.081 | 0.389 | – 0.716 |
| core | *other* | 615 | | 1555 | | 0.712 | |

$$\theta = \pm\left[140\frac{|K_{II}|}{K_I+|K_{II}|+|K_{III}|} - 70\left(\left|\frac{K_{II}}{K_I+|K_{II}|+|K_{III}|}\right|\right)^2\right], \tag{6}$$

where $\Delta K_I$, $\Delta K_{II}$ and $\Delta K_{III}$ are the Modes I, II and III stress intensity factor ranges, and $K_I$, $K_{II}$ and $K_{III}$ are the Modes I, II and III stress intensity factors.

## RESULTS AND DISCUSSION

The maximum contact force was calculated with the inhouse developed program SDAL [25] which is based on the calculation procedure described above. The geometry of the analysed bearing was as follows: the ball track diameter $d_0 = 2010\,\text{mm}$, ball diameter $d_b = 45\,\text{mm}$, osculation $S = 0.97$, nominal contact angle $\alpha = 45°$, and the number of balls $n = 123$. Material properties were: Young's modulus of the rings $E_r = 205000\,\text{MPa}$, Young's modulus of the balls $E_b = 210000\,\text{MPa}$, and Poisson's ratios of the rings and balls $\nu_r = \nu_b = 0.3$. The maximum external load was moment acting about the $x$ axis $M_x = 3214\,\text{kNm}$, and the minimum external load represented unloaded state. These values resulted in the load distribution as shown in Figure 2, and in the maximum contact force and pressure $Q_{max} = 78.93\,\text{kN}$ and $p_{max} = p_0 = 3000\,\text{MPa}$, respectively. The contact ellipsis semi-axis were $a = 10.97\,\text{mm}$ and $b = 1.15\,\text{mm}$.

The curvature radii, which were required for the finite element geometry model were $r_x = r_c = 23.2\,\text{mm}$ and $r_y = 1398.8\,\text{mm}$. As mentioned above, the raceway has been divided into 3 layers: case, transition and core. Each layer had different material properties, which are given in Table 1. The Poisson's ratios for all layers were $\nu = 0.3$. The contact load was simulated as the surface pressure defined by the equation (4), and the coefficient of friction on the raceway was $\mu = 0.05$ [2]. Furthermore, the coefficient of friction between the crack faces was $\mu = 0.5$ [10].

The subsurface stresses and strains, which were calculated in the global model are shown in Figures 6 and 7. The figures show that the stresses reach maximum approximately 0.8 mm under the surface. Thus, an assumption was made, that the subsurface crack appears at this depth. It can also be seen that shear stresses ( $s_{xy}$, $S_{xz}$,

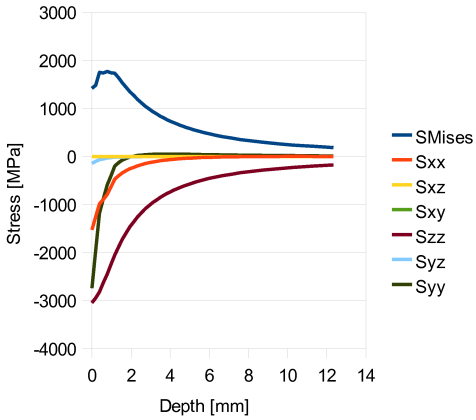


Figure 6. Subsurface stresses at maximum contact pressure

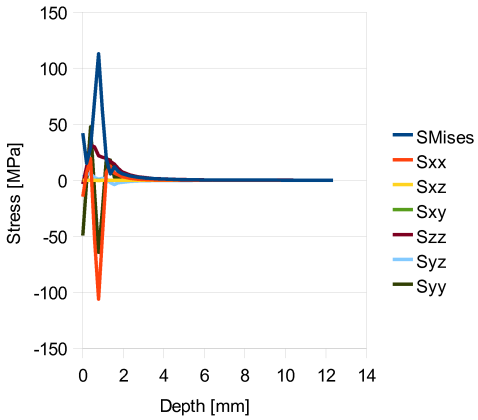


Figure 7. Subsurface (residual) stresses after unloading

$S_{yz}$) are significantly smaller than normal stresses ($S_{xx}$, $S_{yy}$, $S_{zz}$). Only $S_{yz}$, which is due to the Coulomb's friction on the raceway surface. Figure 7 shows the residual stresses after unloading. This means that the plastic deformation under the surface occurred. High scatter of stress values along the crack depth in Figure 7 means that the mesh was too coarse.

In the next step the crack intensity factors and ranges were to be calculated. However, due to problems with the mesh density and the limitations of the current design of the submodel, their values were not calculated accurately enough. Namely, the crack intensity factors were calculated on different crack fronts, but their values on subsequent crack fronts varied too much.

## CONCLUSION

The numerical analysis presented in the paper tries to cover two aspects of the subsurface crack propagation in the large slewing rolling bearings. The first part covers the computation of the maximum contact force acting on the raceway, and the second part covers the computation of the subsurface stresses and strains, and evaluation of the subsurface crack propagation.

The calculation of the maximum contact force is done on the basis of the Hertzian contact pressure. The computational procedure is implemented in the *inhouse* developed program SDAL [25]. Currently the program supports the calculation of single row ball bearings, but this will be enhanced in near future.

The subsurface crack propagation is evaluated by means of finite element analysis. Unfortunately, there was not enough time to improve the finite element model and submodel. Thus, the results obtained by the current model are not good enough, and are not presented in this paper. The reason for such results seams to originate from the mesh density. Since the whole model is entirely parametrised it takes quite some time and effort to enhance it in a way that finer meshes with sufficient quality can be used.

Hence, in near future the finite element analysis will be enhanced, so that the stress intensity factors and ranges can be computed and used in further studies.

## REFERENCES


1. Guideline DG03 - Wind Energy Design: Yaw & Pitch Rolling Bearing Design Life (2000), National Renewable Energy Laboratory.
2. Harris, T.A. (1991) *Rolling Bearing Analysis*, John Wiley & Sons.
3. Zupan, S. and Prebil, I. (2001) *Mechanism and Machine Theory* **36**, 1087–1103.
4. Amasorrain, J. I., Sagartzazu, X. and Damián, J. (2003) *Mechanism and Machine Theory* **38**, 479–496.
5. Ringsberg, J. W., Loo-Morrey, M., Josefson, B. L., Kapoor, A. and Beynon, J. H. (2000) *Int. J. Fatigue* **22**, 205–215.
6. Ringsberg, J. W. and Lindbäck, T. (2003) *Int. J. Fatigue* **25**, 547–558.
7. Ringsberg, J. W. (2005) *Wear* **258**, 955–963.
8. Liu, Y., Stratman, B. and Mahadevan, S. (2006) *Int. J. Fatigue* **28**, 747–756.
9. Liu, Y., Liu, L. and Mahadevan, S. (2007) *Eng. Fract. Mech.* **74**, 2659–2674.
10. Murakami, Y., Fukushima, Y., Toyama, K. and Matsuoka, S. (2008) *Eng. Fract. Mech.* **75**, 306–318.
11. Alfredsson, B. (2000) PhD Thesis, Royal Institute of Technology, Sweden.
12. Glodež, S., Šraml, M. and Kramberger, J. (2002) *Int. J. Fatigue* **24**, 1013–1020.
13. Alfredsson, B. and Cadario, A. (2004) *Int. J. Fatigue* **26**, 1037–1052.
14. Fajdiga, G., Glodež, S. and Kramar, J. (2007) *Wear* **262**, 1217–1224.
15. Glodež, S., Potočnik, R., Flašker, J. and Zafošnik, B. (2008) *Eng. Fract. Mech.* **75**, 880–891.
16. Kida, K., Yamazaki, T., Shibata, M., Oguma, N. and Harada, H. (2004) *Fatigue Fract. Eng. Mater. Struct.* **27**, 481–493.
17. Kida, K., Yoshidome, K., Yamakawa, K., Harada, H. and Oguma, N. (2006) *Fatigue Fract. Eng. Mater. Struct.* **29**, 1021–1030.
18. Olver, A. (2005) In: *Proceedings of the Institution of Mechanical Engineers, Part J: Journal of Engineering Tribology* **219**, 313–330.
19. Kim, T. H. and Olver, A. V. (2001) *Tribology Transactions* **44**, 583–590.
20. Potočnik, R., Flašker, J. and Glodež (2008) In: *Multilevel approach to fracture of materials, components and structures*, pp. 1887–1894, S. Pokluda, J. (Ed.), Czech Chapter, Brno.
21. Stephens, R. I., Fatemi, A., Stephens, R. P. and Fuchs, H. O. (2001) *Metal Fatigue in Engineering (Second Edition)*, John Wiley & Sons.
22. Bauccio, M. (1993) *ASM Metals Reference Book*, ASM International.
23. Socie, D. F. (October, 2008) *Fatigue Calculator*, http://www.fatiguecalculator.com.
24. Pook, L. (2007) *Metal Fatigue: What It Is, Why It Matters*, Springer.
25. Potočnik, R. (2008) *SDAL – A programme for static and dynamic analysis of large slewing bearings*, Faculty of Mechanical Engineering, University of Maribor, Slovenia.